ECS Transactions, 85 (12) 31-40 (2018)
10.1149/08512.0031ecst ©The Electrochemical Society

From Salt to Germanene: A Cookbook for Electrochemical Formation of 2D Materials (Inspired by R. Adžić)

J. Drnec[a], J. L. Stickney[b], and D. A. Harrington[c]

[a] European Synchrotron Radiation Facility, Grenoble, France
[b] University of Georgia, Athens, Georgia, USA
[c] University of Victoria, Victoria BC, Canada

2D materials with honeycomb lattices are increasingly studied due to their unique electronic and mechanical properties. The typical preparation techniques, such as chemical vapor deposition and cleavage of bulk crystals, are either complicated or limited to only certain classes of materials. Here we discuss basic ordering principles in 2D monoatomic layers and show that electrochemical deposition can also result in 2D films with desired honeycomb structures. The principles are first studied on model ionic 2D layers prepared in ultrahigh vacuum. Two ordering possibilities are identified: a bilayer structure for covalently bonded films and a mixed monolayer structure for ionically bonded films. Typically, the most energetically favorable configuration in mixed layers is when ions with one polarity are closely surrounded by ions of the opposite polarity. This translates into a layer with honeycomb structure on substrates with p6/p3 symmetry. This phenomenon can be used to prepare germanene, a layer with such a structure.

Introduction

The re-discovery of graphene, until now the most studied 2D material, opened a large playground for scientists to study exotic properties of confined electrons (1). A few monolayers thick 2D sheets of insulating or semiconducting materials with various atomic compositions rapidly became a hot topic (2). Such sheets were shown to behave differently compared to their 3D counterparts, in large part due to the different electronic structure arising from the 2D nature of the material. They bear great promise for applications in electronics and optoelectronics, sensors, composite materials, photovoltaics, medicine, quantum dots, energy storage and cryptography. The most renowned 2D material is certainly graphene, but its analogs silicene, germanene, stanene and phosphorene have also drawn increased attention due to their potentially simpler incorporation in current semiconductor electronics (3).

There are several means of preparation for 2D materials: exfoliation or cleavage, chemical vapor deposition (CVD) and, as recently shown, also by underpotential deposition (UPD) (3-5). Because standard UPD of transition metals also effectively results in formation of 2D layers, it might therefore be possible to explain the recently observed electrochemical formation of germanene by principles discovered by R. Adžić

and coworkers regarding UPD growth (6). They suggested that depending on the nature of the bond within the binary 2D layer (ionic vs. covalent) one can perhaps predict the general 2D structure of the layer.

As an example, hexagonal structures with various stoichiometries were found when halides were coadsorbed with Tl on an Au(111) electrode in an aqueous environment (6-8). The layers were either mixed monolayers or bilayers, depending on the size of the halogen atoms. The observed mixed monolayer or "coplanar" layers (Fig. 1 left) were rationalized in terms of 2D ionic crystals with moderate substrate influence, where both halogen and Tl atoms were partially charged.

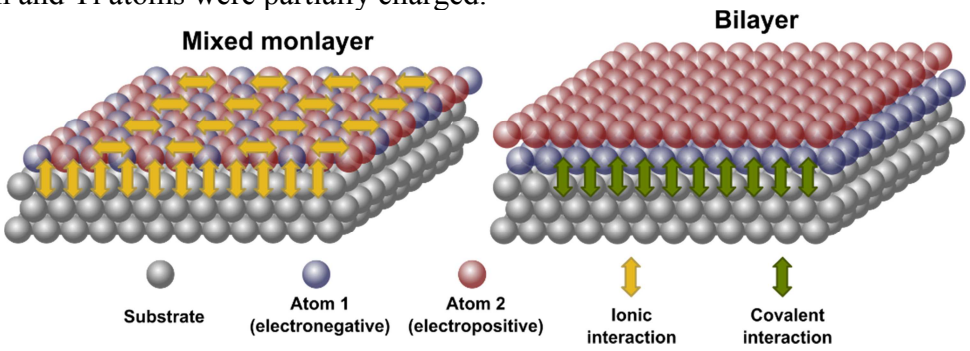

Figure 1. The mixed monolayer and bilayer structures found for bimetallic layers deposited on (111) surfaces. The observations were rationalized by the nature of the bonding within the system: ionic bonding results in a mixed monolayer while covalent bonding results in a bilayer.

The authors proposed that 1:1, 1:2 and 1:3 stoichiometries are the most favorable for 2D binary ionic layers because they maximize the interactions between adjacent oppositely-charged ions. The coplanar structure was also found by Labayen and Harrington when Tl and I were electrodeposited on a Pt(111) surface (9). The experimental findings of Cs and I coadsorption on an Au(110) surface performed by Wang et al. showed similar behavior: Cs and I ions formed a coplanar structure with a quasi-square symmetry (10). In the studies of AgI layers electrodeposited on Pt(111), Labayen and Harrington rationalized the structure of the adlayer in terms of covalent bonding within the layer (11-12). They suggested that the covalent characteristic of an Ag-I bond is responsible for an AgI bulk-like bilayer surface structure. The studies mentioned above suggest that the structure of binary layers has either a bilayer or planar character depending on the bonding type. For surfaces where the bond between the adsorbates is covalent, the predicted structure is a bilayer. For layers where bonds between adsorbates are predominantly ionic, the predicted structure is a mixed monolayer.

Results and discussion

To further test the proposed hypothesis, we prepared binary layers from highly electropositive cesium and electronegative iodine or oxygen deposited on Pt(111) (13,14). According to the previous observations, the resulting ionically bonded layers are expected to have a mixed monolayer structure. These layers were prepared in UHV conditions (10^{-10} mbar base pressure) in order to minimize the influence of the surrounding electrolyte and to better control the preparation process. The use of alkali metal and halogen is necessary to assure that the resulting layer will be as ionic as

possible because the previous work typically used binary systems consisting of transition metal and halogens, where the ionicity of the bonding is less guaranteed due to the smaller difference in electronegativity.

The first step in the preparation process is the deposition of Cs on Pt(111) from a getter material (SAES getters). The typical work function (WF) response, together with the Low Energy Electron Diffraction (LEED) patterns and real space structures, is shown in Fig. 2 (15).

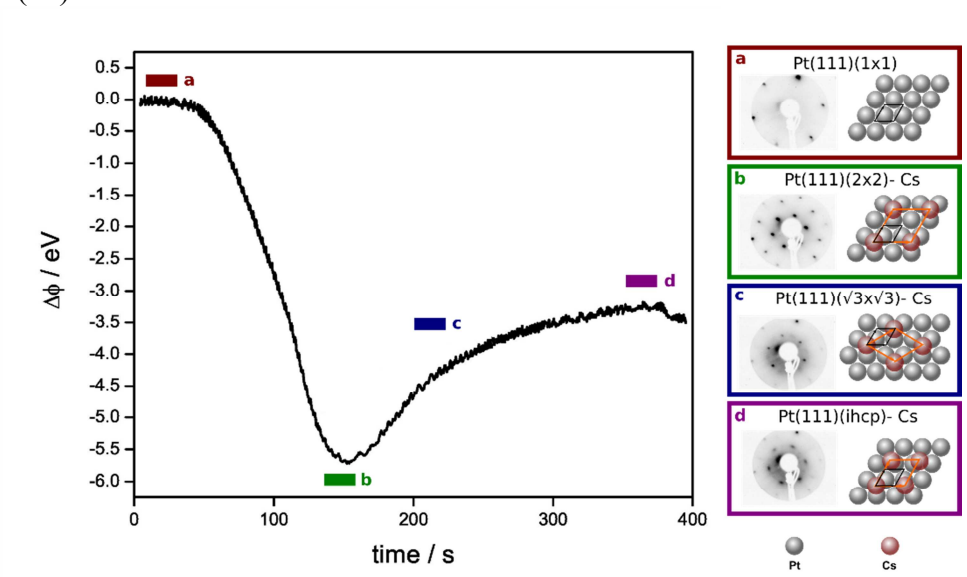

Figure 2. The work function (WF) response upon Cs adsorption on Pt(111) in UHV conditions. The WF first drops significantly to the minimum corresponding to the (2×2) LEED pattern. Upon further dosing the WF increases and the LEED pattern changes to (√3×√3)-*R*30°. The maximum Cs coverage corresponds to an incommensurate hexagonal close packed (ihcp) structure. The real space structures are shown on the right side together with the LEED patterns.

First, the WF drops significantly by –5.5 eV when compared to the bare Pt surface. At the minimum of the WF we observe Pt(111)(2×2)-Cs (Cs coverage θ_{Cs}=0.25) structure which then evolves through Pt(111)(√3×√3)-*R*30°-Cs (θ_{Cs}=0.33) to the Cs saturated surface. At saturation the surface is covered by a hexagonal close packed incommensurate Cs layer (Pt(111)(ihcp)-Cs) with the work function change about –3.5 eV compared to the initial bare Pt surface, and Cs coverage of 0.41 as determined by Auger Electron Spectroscopy (AES).

To prepare the CsI mixed layer we further dosed iodine on Cs saturated (Pt(111)(ihcp)-Cs) surface from a Ag_4RbI_5 solid state electrochemical cell (Fig.3) (13,16).

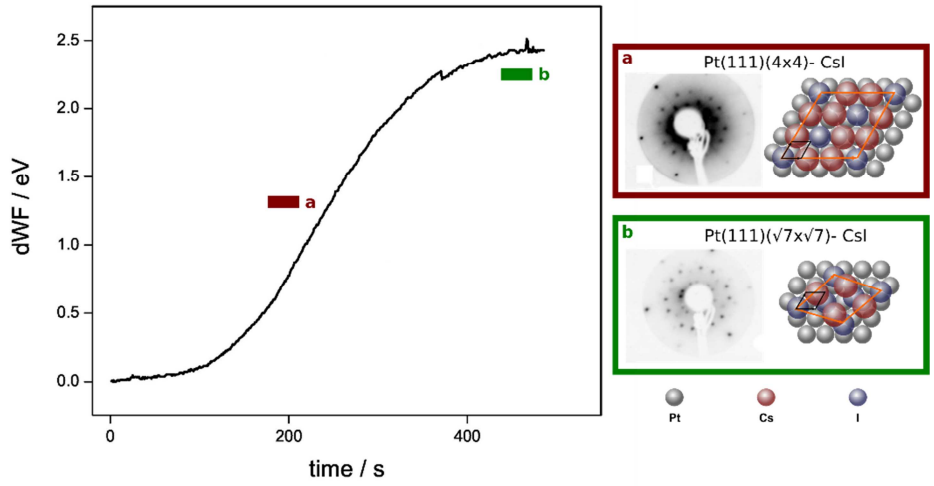

Figure 3. The work function (WF) response upon I dosing Cs saturated on Pt(111)(ihcp)-Cs in UHV conditions. The WF steadily rises by 1.5 eV from the initial value. The LEED pattern changes through (4×4) to (√7×√7)-*R*19.1° at the Cs and I saturated surface. The real space structures are shown on the right side together with the LEED patterns.

Incorporation of I into the Cs layer causes the WF to increase due to the introduction of charge of opposite polarity into the structure. After reaching the desired WF change corresponding to a certain CsI coverage, the surface was briefly annealed to 350 K to enhance the layer ordering. The LEED pattern changes from Pt(111)(ihcp)-Cs present at the beginning of the I dose to a Pt(111)(4×4)-Cs,I pattern which corresponds to a WF change of about 1 eV. After further I dosing the pattern changes to Pt(111)(√7×√7)-*R*19.1°-Cs,I. The coverages of then ordered layers were determined by Auger Electron Spectroscopy (AES) as θ_{Cs}=0.35±0.11, θ_I=0.28±0.07 for Pt(111)(4×4)–Cs,I and θ_{Cs}=0.33±0.07, θ_I=0.35±0.06 for Pt(111)(√7×√7)-*R*19.1°-Cs,I (13). Given the high packing density of the Pt(111)(√7×√7)-*R*19.1°-Cs,I structure, it is likely that this layer is a bilayer where the I atoms are in contact with the Pt substrate and the Cs atoms are located on top of the stack as schematically depicted on the right side of Figure 1.

More interesting for further discussion is the Pt(111)(4×4)–Cs,I layer where the packing allows accommodation of all atoms in one monolayer, forming the mixed monolayer structure. However, more than one packing order is possible for a structure with hexagonal symmetry (13). The possibilities are shown in Figure 4.

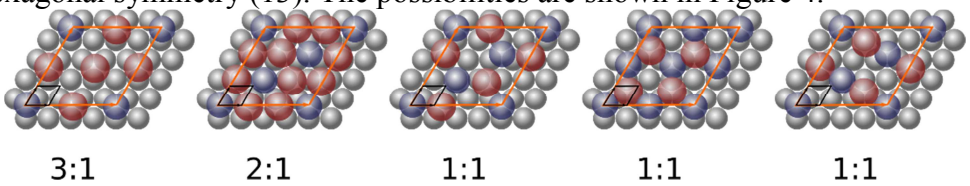

Figure 4. Possible Pt(111)(4×4)–Cs,I structures of various Cs:I stoichiometries for mixed CsI monolayers.

Based on the symmetry and AES measured coverages, we concluded that the most probable atomic arrangement of the Pt(111)(4×4)–Cs,I structure is the one depicted second from the left in Figure 4 (7,13). In this arrangement the Cs:I ratio is 2:1 and each I atom is surrounded by the maximum number of Cs counterions. According to the LEED

and thermal desorption measurements, the surface is not only covered by this structure, but a significant area is also covered by high iodine coverage structures (13).

The fact that the ionic layers organize into very defined arrangements is not a surprise, as suggested by standard electrostatic calculations taking into the account the image charges in the metal substrate (7,13). These calculations show that, depending on the electrostatic charge of each atom and on the distance from the surface, only a few surface stoichiometries are favorable, namely Cs_2I and CsI where the overall electrostatic energy is minimized.

To check the universality of these observations, we prepared layers consisting of Cs and oxygen. For such layers we also expect high ionicity of the bonding given the large electronegativity difference between Cs and oxygen. The structures were prepared by oxidation of the fully saturated Pt(111)(ihcp)-Cs structure at $5x10^{-8}$ mbar of oxygen pressure. Such layers initially show no obvious order, but a clear Pt(111)(4×4)–Cs,O LEED pattern appeared after annealing to 650 K (14). Similar to the CsI case and after taking into the consideration the stoichiometry of the surface layer measured by AES, the surface can be the best described by the structure where the anions (oxygen) are surrounded by the maximum number of cations (cesium) in a closely packed arrangement (Figure 5).

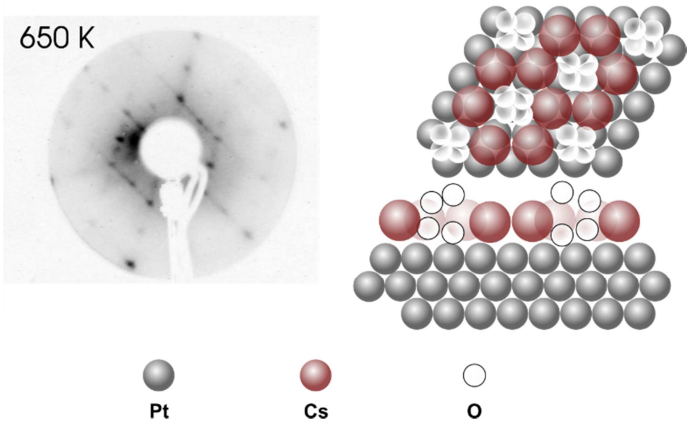

Figure 5. The LEED pattern and the proposed structure for the Pt(111)(4×4)–Cs,O prepared by exposing the Pt(111)(ihcp)-Cs structure to 5×10^{-8} mbar oxygen pressure and annealing to 650 K.

Such honeycomb arrangements are not only specific to the above-mentioned coadsorption systems prepared in UHV conditions. The (4×4) LEED patterns and mixed layer structures were also observed for CsI layers prepared by electrochemical deposition on Au(111) (17), and KO deposits on Pt(111) prepared in UHV (18). Even though here we consider only the (111) surface orientation of a f.c.c. crystal lattice, the same principles have been proposed to govern the coadsorption for other symmetries. The same general behavior was also observed for Cs and I coadsorption on Au(110) electrodes in electrochemical conditions (19-20). At low potentials, the mixed Au(110)(2×4)-Cs,I structure was observed and the model favored by Wang et al. has a planar, mixed layer with 1:1 stoichiometry and atomic spacing almost identical to that in the bulk CsI crystal (20). In this case the ions of one polarity are also surrounded by maximum numbers of counterions in the four-fold symmetry arrangement. Given the above, it seems that there is now a significant body of knowledge justifying the

hypothesis made by Wang et al. and Drnec and Harrington regarding the nature of the bonding and structure of 2D layers. The honeycomb arrangement observed for the (111) surfaces is interesting as it is the same, for one of the ionic species, as the arrangement of graphene and other materials with sp^2 or mixed sp^2-sp^3 hybridization. Such materials hold much promise given the unique properties leading to interesting electronic, optical and mechanical behavior. The examples of such materials are graphene, silicene, germanene and stanene (1,21-23).

This raises a question if the universality of the structure-bonding relationship for ionic layer cannot be translated into the preparation of advanced 2D materials with honeycomb lattices. According to the hypothesis it should be possible to imprint the honeycomb structure during the deposition of arbitrary atomic species on the six-fold symmetry substrate. However, two basic conditions need to be satisfied: i) the interaction of the deposited film with the metallic substrate is relatively weak or at least non-directional (ionic or van der Waals bonding) and ii) the deposition proceeds from the environment where the deposited atoms are present in an ionic state together with ions of opposite polarity. The electrochemical environment is almost an ideal deposition medium as the depositing material is normally surrounded by the counterions in the ion-conducting electrolyte. In the double layer region there is typically enough mobility that the ions can organize in the precursor state, as in the case of $[PdCl_4]^{2-}$ complexes on Au(111) prior to the Pd deposition (24). Such an organized precursor state, together with the driving electric field from induced image charges on the metallic surface, can serve as a template for further deposition. This process can facilitate formation of certain structures, in this case the honeycomb structure, as depicted in Figure 6.

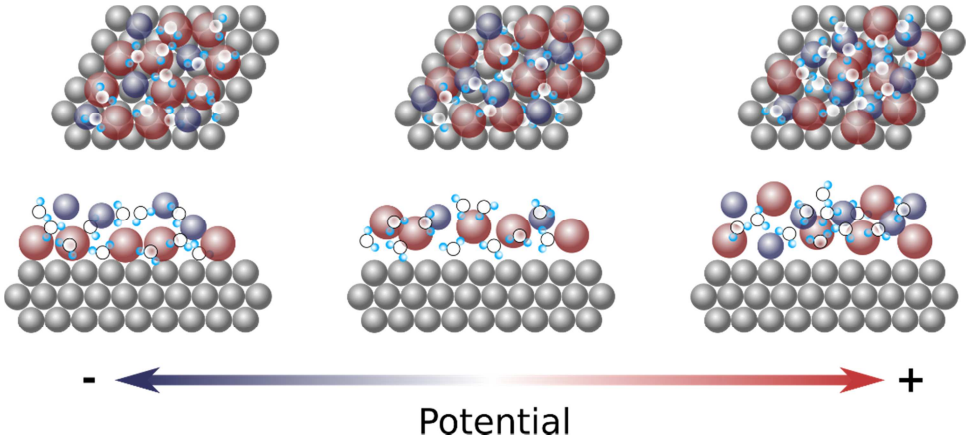

Figure 6. Hypothesis: The deposition of the honeycomb structure proceeds from the precursor state formed in the double layer at the potentials higher than the deposition potential. Firstly, the ions in double layer are disordered (right) at potentials higher than the deposition potential. Upon sweeping the potential negatively towards the deposition potential, the ions organize in the ordered precursor state (middle). Finally, the positive ionic species deposit on the substrate from the ordered precursor state (left).

Above the deposition potential (right scheme in Figure 6) the double layer (DL) consists of a disordered mix of ions of opposite polarity and water molecules. As the potential decreases to the UPD potential, cations move closer to the surface, possibly interacting with the substrate through ionic and van der Waals interactions. This, together

with the presence of the anions, forces the cations to assemble in the DL into the favorable structure, which in the case of p3/p6 symmetry of the substrate is the honeycomb (Figure 6 middle). Upon further potential decrease, the cations specifically adsorb on the surface from the precursor state (Figure 6 left). If the adsorbed atoms interact with the substrate ionically or this bond is weak, e.g., van der Waals, then the adsorbed layer keeps its structure. If there is a strong covalent bonding, then the structure reorganizes to the typical UPD closely packed layer (6).

Following this hypothesis, we tried to deposit germanium on Au(111) substrate in order to form germanene, the analog for graphene with the honeycomb lattice (4-5). This structure cannot be formed by exfoliation as there is no Ge analog to graphite, where 2D sheets are hold together by the van der Waals forces. The last monolayer of the Au(111) substrate has p6 symmetry, as for Pt(111), but it has a large herringbone reconstruction. The lattice parameter is such that it matches the atomic distances of the theoretically calculated germanene honeycomb lattice, therefore it is ideal for germanene formation. Even though various groups have tried to deposit germanene in the UHV environment in the past, only in recent years there has been success (25-31).

We found that it is possible to form germanene from aqueous electrolyte by finely tuning the deposition conditions (4). In the case of Au(111) at pH 4.5, the reconstruction is first lifted by incorporation of some of the Ge atoms into the substrate, forming a surface alloy. This alloy releases the surface stress and the unreconstructed (111) surface is formed, which then acts as a better template for the deposition of the germanene. The substrate effects seems to be dependent on the deposition conditions and pH because at pH 9 the germanene also forms on the reconstructed Au(111) surface (5). A specific potential control procedure needs to be applied to form the germanene 2D layer (Figure 7). Such deposited germanene shows many defects. However, fine tuning of the deposition conditions helps to form less defective layers. Deposition at other conditions results in less well ordered 2D deposits and surface alloys. According to the hypothesis this is not surprising as fine potential control is likely required in order to form the ordered precursor state.

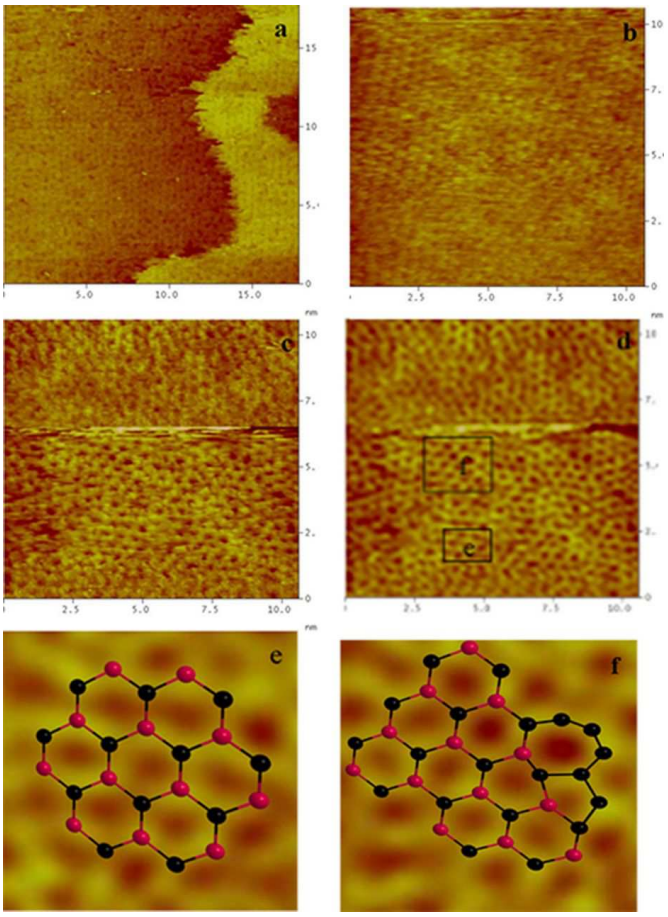

Figure 7. a-f (left to right) are STM images of Au(111) in 1 mM GeO_2 and 0.1 M $KClO_4$ (pH 4.2) after the potential was scanned to −1.4 V and then to −900 mV vs. Ag/AgCl. a) shows a strip of germanene on a layer of germanene. b) shows a honeycomb structure, with 0.44 ± 0.02 nm between the holes. c) shows nearly atomically resolved germanene. The boxes indicate where figures e and f were taken. e) Superposition of honeycomb structure and a FFT-filtered STM image of a germanene domain. f) Superposition of a germanene model, including 5- and 7-membered rings at a domain wall, on a FFT-filtered germanene STM image. Reproduced with permission from *J. Electrochem. Soc.*, **164** (2017), D469-D477. Copyright 2017, The Electrochemical Society.

At pH 9 a buffer solution can be used and the process can be better controlled due to the shift of the hydrogen evolution reaction to lower potentials and better control of the surface pH. Here germanene growth on both reconstructed and unreconstructed surfaces was observed, but the growth was accelerated on the unreconstructed part of the surface. This is again presumably due to the better templating effects for the deposition. Stepping out of the ideal growth conditions results in less well ordered germenene, as in the pH 4.5 case. This is expected from the hypothesis, where the right conditions need to be found to preassemble the monolayer in the precursors state.

Conclusions

Above we have shown that the nature of the bonding and the symmetry of the substrate determine the structure of (electro)deposited atomically thin bimetallic layers. In the case of a substrate with the hexagonal symmetry, ionically bonded layers form a honeycomb planar structure where ions of one polarity are surrounded by maximum ions of opposite polarity. This behavior can be explored in preparation of 2D materials with honeycomb structures, such as germanene, in an aqueous environment, where the deposited atomic species exist in an ionic form surrounded by counterions. Given the above observations, it is perhaps feasible to expect that the same phenomena will direct the deposition of other exotic 2D materials which are non-directionally bonded to the substrate. For example, silicon has been shown to deposit from ionic liquids at various conditions on the Au(111) surface (32). Given that silicene is a stable allotrope of silicon, it is not unreasonable to expect silicene formation on one of the transition metals, e.g., Au(111), in electrochemical conditions. The same might be expected for carbon deposition from CH_4 or CO, where by finely tuning the conditions, it might be possible to prepare graphene at room temperature. Such an approach might be also used to prepare as-yet-unknown 2D materials.

Acknowledgments

The authors thank the Natural Sciences and Engineering Research Council of Canada for funding, the European Synchrotron Radiation Facility for providing beam time, and the ID03 beamline staff for help with the experiments.

References

1. K. S. Novoselov, A. K. Geim, S. V. Morozov, D. Jiang, Y. Zhang, S. V. Dubonos, I. V. Grigorieva, A. A. Firsov, Science, 306, 666–669 (2004).
2. R. F. Service, Science, 348, 490-492 (2015).
3. S. Balendhran, S Walia, H. Nili, S. Sriram and M. Bhaskaran, Small, 11, 640–652 (2015).
4. M. Ledina, N. Bui, X. Liang, Y. -G. Kim, J. Jung, B. Perdue, C. Tsang, J. Drnec, F. Carla, M.P. Soriaga, T. J. Reber, J. L. Stickney, J. Electrochem. Soc. 164, D469-D477 (2017).
5. N. N. Bui, M. Ledina, T. J. Reber, J. Jung, and J. L. Stickney, ACS Nano, 11, 9481−9489 (2017).
6. J. X. Wang, I. K. Robinson, J. E. DeVilbiss and R. Adžić, J. Phys. Chem. B, 104, 7951–7959 (2000)
7. J. X. Wang, I. K. Robinson, and R. R. Adzic, Surf. Sci., 412-413, 374-383 (1998).
8. R. R. Adzic and J. X. Wang, J. Phys. Chem. B, 102(33), 6305-6308 (1998).
9. M. Labayen and D. A. Harrington, J. Electroanal. Chem., 567, 185-192 (2004).
10. J. Wang, G. Watson, and B. Ocko, J. Phys. Chem., 100(16), 6672-6677 (1996).
11. M. Labayen and D. A. Harrington, J. Electroanal. Chem., 583(1), 77-83 (2005).
12. M. Labayen, D. A. Harrington, M. Saidy, and K. A. Mitchell, Surf. Sci., 490, 256-264 (2001).
13. J. Drnec and D. A. Harrington, Surf. Sci., 604, 2106–2115 (2010).
14. J. Drnec and D. A. Harrington, Surf. Sci., 630, 9-15 (2014).

15. J. Drnec and D. A. Harrington, Surf. Sci., 603(13), 2005-2014 (2009).
16. S. A. Furman and D. A. Harrington, J. Vac. Sci. Technol., A, 14, 256-257 (1996).
17. B. G. Bravo, S. L. Michelhaugh, M. P. Soriaga, I. Villegas, D. W. Suggs, and J. L. Stickney, J. Phys. Chem., 95, 5245–5249 (1991).
18. E.L. Garfunkel, G.A. Somorjai, Surf. Sci., 115, 441 (1982).
19. X. Gao, G. J. Edens, F.-C. Liu, M. J. Weaver, and A. Hamelin, J. Phys. Chem., 98, 8086–8095 (1994).
20. J. Wang, G. Watson, and B. Ocko, J. Phys. Chem., 100, 6672–6677 (1996).
21. S. Cahangirov, M. Topsakal, E. Aktürk, H. Sahinand S. Ciraci, Phys. Rev. Lett., 102, 236804 (2009).
22. Feng Zhu, W. Chen, Y. Xu, Ch. Gao, D. Guan, C. Liu, D. Qian, S. Zhang and J. Jia, Nat. Mater., 14, 1020–1025 (2015).
23. F. Matusalem, D. S. Koda, F. Bechstedt, M. Marques and L. K. Teles, Sci. Rep., 7, 15700 (2017).
24. L.A. Kibler, M. Kleinert, R. Randler and D.M. Kolb, Surf. Sci., 443, 19-30 (1999).
25. L. Li, S.-z. Lu, J. Pan, Z. Qin, Y.-q. Wang, Y. Wang, G.-y. Cao, S. Du and H.-J. Gao, Advanced Materials, 26, 4820 (2014).
26. M.E. Davila, L. Xian, S. Cahangirov, A. Rubio and G. Le Lay, New J. Phys., 16, 095002/1 (2014).
27. M.E. Davila and G. Le Lay, Sci. Rep., 6, 20714 (2016).
28. P. Bampoulis, L. Zhang, A. Safaei, R. van Gastel, B. Poelsema, H.J.W. Zandvliet, J. Phys.: Condens. Matter, 26, 442001/1 (2014).
29. H.-S. Tsai, Y.-Z. Chen, H. Medina, T.-Y Su., T.-S. Chou, Y.-H. Chen, Y.-L. Chueh and J.-H. Liang, Phys. Chem. Chem. Phys., 17, 21389 (2015).
30. F. d'Acapito, S. Torrengo, E. Xenogiannopoulou, P. Tsipas, J.M. Velasco, D. Tsoutsou and A. Dimoulas, Journal of Physics-Condensed Matter, 28, 045002 (2016).
31. E. Bianco, S. Butler, S. Jiang, O.D. Restrepo, W. Windl and J.E. Goldberger, ACS Nano, 7, 4414 (2013).
32. N. Borisenko, S. Zein El Abedin and F. Endres, J. Phys. Chem. B, 110, 6250–6256 (2006).